Three-dimensional model for the effective viscosity of bacterial suspensions

Brian M. Haines,[1] Andrey Sokolov,[2,3] Igor S. Aranson,[3] Leonid Berlyand,[1] and Dmitry A. Karpeev[4]
[1]*Department of Mathematics, Penn State University, McAllister Bldg, University Park, Pennsylvania 16802, USA*
[2]*Illinois Institute of Technology, 3101 South Dearborn Street, Chicago, Illinois 60616, USA*
[3]*Materials Science Division, Argonne National Laboratory, 9700 South Cass Avenue, Argonne, Illinois 60439, USA*
[4]*Mathematics and Computer Science Division, Argonne National Laboratory, 9700 South Cass Avenue, Argonne, Illinois 60439, USA*
(Received 13 May 2009; revised manuscript received 15 September 2009; published 22 October 2009)

We derive the effective viscosity of dilute suspensions of swimming bacteria from the microscopic details of the interaction of an elongated body with the background flow. An individual bacterium propels itself forward by rotating its flagella and reorients itself randomly by tumbling. Due to the bacterium's asymmetric shape, interactions with a prescribed generic (such as planar shear or straining) background flow cause the bacteria to preferentially align in directions in which self-propulsion produces a significant reduction in the effective viscosity, in agreement with recent experiments on suspensions of *Bacillus subtilis*.

DOI: 10.1103/PhysRevE.80.041922 PACS number(s): 87.16.−b, 05.65.+b

Recently, there has been much interest in studying the dynamical properties of interacting self-propelled organisms such as flocking birds, schooling fish, and swarming bacteria [1–6]. Such systems, relying on nonlocal interactions, exhibit collective behavior absent from passive systems, such as suspensions of inert particles. Experiments on bacteria suspended in liquid films have demonstrated enhanced diffusion of tracer particles [1] and collective flow speeds that exceed the speed of an individual bacterium by an order of magnitude [7]. In our experiments (detailed in [8]), the swimming of suspensions of *Bacillus subtilis* was observed to cause a decrease in the effective viscosity by an order of magnitude. Whereas phenomenological arguments relating the viscosity of suspensions to the activity of particles [9], studies of viscosity in two-dimensional geometry [10], and numerics [11,12] have been presented, the issue of viscosity in suspensions of swimmers still lacks conceptual clarity. In [9], a phenomenolgical order parameter is used to characterize the local ordering of the system (i.e., the local alignment of swimming particles). The relationship of the evolution of the order parameter to the microscopic alignment dynamics was not clarified, and the very possibility of arriving at macroscopic expressions for the effective viscosity from first-principles arguments was not established.

In this paper, we study the rheology of dilute suspensions of swimming bacteria. In the dilute regime (when the volume fraction $\phi \lesssim 2\%$), bacteria interact only with the background flow and not with each other, simplifying the problem dramatically. Nevertheless, producing an adequate model has proved challenging. Numerical simulations in [11] using spherical bacteria with imposed boundary velocities modeling self-propulsion were able to predict a decrease in the effective viscosity only in the presence of a gravitational field. In [10], modeling bacteria as self-propelled disks (where drag on the flagellum is neglected), we obtained an asymptotic expression for the effective viscosity in terms of a given orientation distribution function P. This showed that there is a decrease in the effective viscosity due to self-propulsion when bacteria align along one of the principal axes of the hydrodynamic rate of strain tensor. This alignment can only be achieved by asymmetric bacteria.

In this work, we significantly generalize and extend the work in [10]. We consider asymmetric bacteria in a three-dimensional geometry and include the effects of tumbling (random reorientation). We have derived analytical expressions for all components of the deviatoric stress tensor along with steady-state orientation distributions for several relevant cases and used these to obtain explicit expressions for the effective viscosity. Most significantly, we base our analysis on microscopic considerations, and, hence, extend and complement the phenomenological theory of nematic ordering. In particular, it is possible from our model to write down the order-parameter equation and provide a rigorous justification for the phenomenological theory presented in [9]. We quantify the dependence of the local ordering and the effective viscosity on the microscopic parameters: the shear rate and vorticity of the flow, as well as the bacterial shape and tumbling rate. The dependence on vorticity has not previously been observed in phenomenological theories.

Our analysis shows a general trend of decreasing effective viscosity with increasing bacterial concentration and activity (speed of swimming). The effect is best demonstrated in Fig. 1 where selected results on experiments with aerobic motile bacteria *Bacillus subtilus* confined in a free-standing liquid film are presented. A detailed account of the experimental work will be reported in the experimental [8]. The viscosity η is inferred from the decay rate ν of a macroscopic vortex of size $L \sim 2$ mm induced in a thin film containing a bacterial suspension by a moving microprobe. The experiments were performed for a broad range of bacterial volume fractions ϕ. As one can see from the Figure, an almost sevenfold drop of the decay rate ν is measured while the density is increased from $\phi=0$ (no bacteria) to $\phi \simeq 2\%$. Since the viscosity $\eta \propto \nu L^2$, this indicates a significant decrease of the viscosity.

Bacteria come in a variety of shapes, including spheres, rods, and spirals and employ many different forms of motility. We consider bacteria similar to the *Bacillus subtilis* used in the experiments in [7]. This is a rod-shaped unicellular microorganism that propels itself through the rotation of several helical flagella distributed throughout its body. It moves in two distinct modes (see, e.g., [13,14]): forward movement (swimming) and tumbling (random reorientation). It spends most of its time moving forward, with its flagella bundled

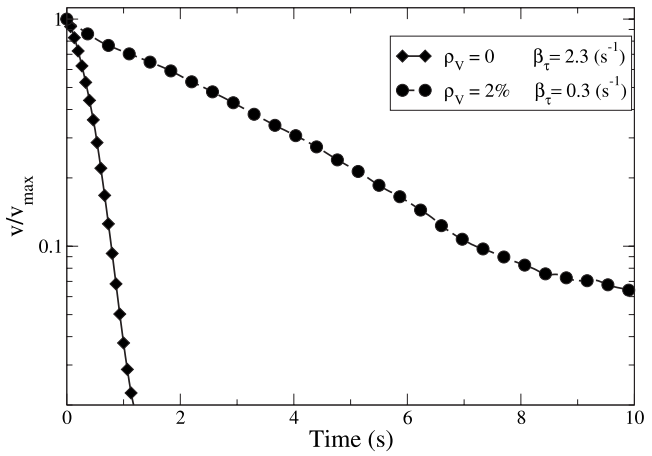

FIG. 1. Semilogarithmic plot illustrating the decay of the typical velocity v of a macroscopic vortex normalized by the maximum velocity $v_{\max}$ for different values of the volume fraction ϕ. The lines show a fit to $v \sim \exp(-\nu t)$. The dashed line with circles corresponds to a fluid without bacteria and the solid line with diamonds corresponds to the suspension with a 2% volume fraction of bacteria.

together so that they rotate as one strand. At random times (depending on conditions, the average time between tumbling events varies from 1 to 60 s; see [14]), the flagella unbundle and rotate separately, causing the bacterium to reorient, until the next bundling event. This effectively results in a random reorientation of the bacterium that can be modeled as a random walk on the unit sphere [15]. It should be noted that not all bacteria are propelled in such a manner, and our results are not expected to hold for bacteria that do not tumble.

We model a bacterium as a rigid prolate spheroid with semiaxes a, b (see Fig. 2) subject to no-slip boundary conditions in a Stokesian fluid of viscosity η whose velocity is denoted by $\boldsymbol{u}$ and pressure by p. The bacterium translates with linear velocity $\boldsymbol{v}$ and rotates with angular velocity $\boldsymbol{\omega}$. On the container boundary, the fluid is subject to boundary conditions $\boldsymbol{u}=E\cdot\boldsymbol{x}+\boldsymbol{\Omega}\times\boldsymbol{x}$, where E is a given symmetric and trace-free matrix and $\boldsymbol{\Omega}$ is a given vector. Self-propulsion is modeled by means of a rigidly attached point force of magnitude c and direction $\hat{\boldsymbol{d}}$ located at $\boldsymbol{x}^f$, displaced by $b(1+\lambda)\hat{\boldsymbol{d}}$ from the center of the bacterium $\boldsymbol{x}^c$. In order to model tumbling, the bacterium exerts a torque τ on the fluid

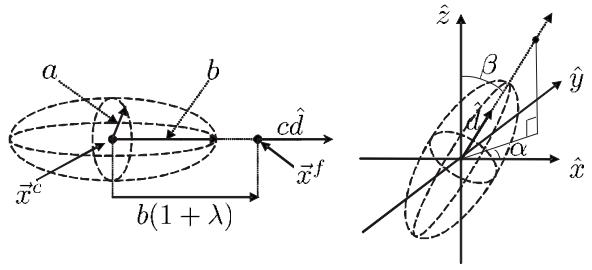

FIG. 2. Schematic representation of a bacterium (left), bacterium with orientation (α,β), alternatively described by the unit vector $\hat{\boldsymbol{d}}$ (right).

selected to make $\dot{\hat{\boldsymbol{d}}}$ contain a white-noise process. The dynamics of each bacterium are determined by enforcing a balance of hydrodynamic forces and torques with those exerted by the bacterium on the water

$$\int_{\partial B} \sigma\cdot\hat{\boldsymbol{n}}dx + c\hat{\boldsymbol{d}} = 0,$$

$$\int_{\partial B} \sigma\cdot\hat{\boldsymbol{n}}\times(\boldsymbol{x}-\boldsymbol{x}^c)dx + \tau = 0, \tag{1}$$

where ∂B is the surface of the bacteria, $\sigma_{ij} := -p\delta_{ij} + 2\eta e_{ij}$ is the stress, and $e_{ij} := \frac{1}{2}(\frac{\partial u_i}{\partial x_j} + \frac{\partial u_j}{\partial x_i})$ is the rate of strain.

In the dilute limit, the fluid problem is posed for a single particle in an infinite domain,

$$\begin{cases} \eta\Delta\boldsymbol{u} = \nabla p + c\hat{\boldsymbol{d}}\delta(\boldsymbol{x}-\boldsymbol{x}^f) & \boldsymbol{x}\in\mathbb{R}^3\setminus B \\ \nabla\cdot\boldsymbol{u} = 0 & \boldsymbol{x}\in\mathbb{R}^3\setminus B \\ \boldsymbol{u} = \boldsymbol{v}+\boldsymbol{\omega}\times(\boldsymbol{x}-\boldsymbol{x}^c) & \boldsymbol{x}\in\partial B \\ \boldsymbol{u}\to E\cdot\boldsymbol{x}+\boldsymbol{\Omega}\times\boldsymbol{x} & \boldsymbol{x}\to\infty \\ \int_{\partial B}\sigma\cdot n dx + c\hat{\boldsymbol{d}} = 0 & \\ \int_{\partial B}\sigma\cdot n\times(\boldsymbol{x}-\boldsymbol{x}^c)dx + \tau = 0 & \end{cases} . \tag{2}$$

We obtained the exact solution to Eq. (2) by taking the Green's function for Stokes' equation and canceling the flow at the surface of the bacterium using Faxén's law for the prolate spheroid (see Appendix). Assuming the bacterium is placed in a background flow described by a constant rate of strain E and vorticity $\boldsymbol{\Omega}$, we plug the hydrodynamic solutions into (1) to obtain the equations of motion for a single bacterium with linear velocity $\boldsymbol{v}=v\hat{\boldsymbol{d}}$ and angular velocity $\boldsymbol{\omega}$:

$$c = 6\pi b\,\eta v N \tag{3a}$$

$$\tau_i = 8\pi\eta b^3[X^C d_i d_j + Y^C(\delta_{ij}-d_i d_j)](\Omega_j-\omega_j) - 8\pi\eta b^3 Y^H \epsilon_{ijm} d_m d_k E_{jk}, \tag{3b}$$

where X^C, Y^C, Y^H are scalar functions of the eccentricity $e = \sqrt{b^2-a^2}/b$ and N is a scalar function of e, λ [16]. X^C, Y^C, Y^H, and N are plotted in Fig. 3.

Since in isotropic media the effective viscosity does not depend on the locations of individual bacteria, we do not need to solve Eq. (3a) explicitly. Introducing $P(\hat{\boldsymbol{d}},t)$, which represents the probability that any bacterium, at time t, has orientation $\hat{\boldsymbol{d}}$, Eq. (3b) leads to the Fokker-Planck equation

$$\frac{\partial P}{\partial t} = -\nabla_{\hat{d}}\cdot(P\dot{\hat{\boldsymbol{d}}}^D) + D\Delta_{\hat{d}}P, \tag{4}$$

where $\Delta_{\hat{d}}$ is the spherical Laplacian, $\nabla_{\hat{d}}$ is the spherical gradient, and $\dot{\hat{\boldsymbol{d}}}^D$ is the deterministic contribution to $\dot{\hat{\boldsymbol{d}}}$ (due to interaction with the background flow only—i.e., the solution of Eq. (3b) with $\tau=0$). We assume the relevant distribution

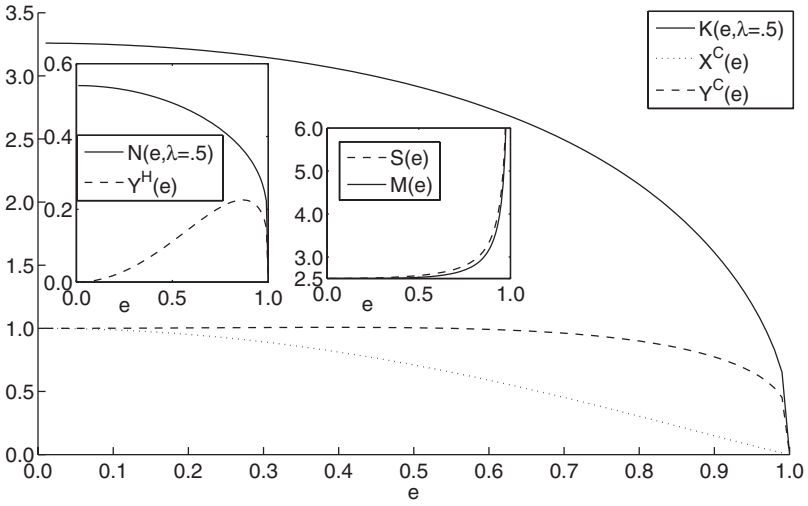

FIG. 3. Various scalar functions of eccentricity $e=\sqrt{b^2-a^2}/b$ and relative distance between body and point force $\lambda := \frac{|x^f-x^c|-b}{b}$.

for calculating bulk quantities is the steady-state distribution P^∞ obtained from Eq. (4) by setting $\frac{\partial P^\infty}{\partial t}=0$.

The bulk deviatoric stress is defined by

$$\Sigma_{ij} := n_V \int_{S^2} \int_V \left(\sigma_{ij}(\hat{\boldsymbol{d}}) - \frac{1}{3}\delta_{ij}\sigma_{kk}(\hat{\boldsymbol{d}}) \right) P^\infty(\hat{\boldsymbol{d}}) dx dS, \quad (5)$$

where n_V is the volume density of bacteria, V is any volume containing the entire suspension (the value of Σ is independent of V), and $\sigma(\hat{\boldsymbol{d}})$ is the hydrodynamic stress due to an inclusion centered at the origin with orientation $\hat{\boldsymbol{d}}$. Plugging in $\boldsymbol{u}$ and p, we obtain our first result (see Appendix),

$$\begin{aligned}\Sigma_{ij} = 2\eta E_{ij} + \phi \Bigg[\frac{b^2}{a^2}\eta \Bigg(5\int_{S^2} \Lambda_{ijkl} P^\infty dS E_{kl} - 3BY^H \int_{S^2} (\epsilon_{ikl} d_j \\ + \epsilon_{jkl} d_i) d_l \epsilon_{kmn} d_m d_n P^\infty dS E_{mn} + 3Y^H D \int_{S^2} (\epsilon_{ikl} d_j \\ + \epsilon_{jkl} d_i) d_l \epsilon_{kmn} d_m (\partial_n P^\infty) dS \Bigg) + \frac{c}{16\pi a^2} K \int_{S^2} (\delta_{ij} \\ - 3 d_i d_j) P^\infty dS \Bigg] + O(\phi^2), \end{aligned} \quad (6)$$

where Λ is a function of shape and orientation and K is a scalar function of e and λ, both given in [16], and $B := \frac{b^2-a^2}{b^2+a^2}$. Plots of Y^C, Y^H, and K are given in Fig. 3. The first term in Eq. (6) is the standard Newtonian stress. The second and third terms are due to the presence of passive spheroids and are taken from [17]. The fourth term is the diffusive stress, obtained from [18]. The last term is due to self-propulsion. Since $K>0$, the sign of the last term is determined by the sign of c ($c>0$ for "pushers") and the distribution of orientations of the bacteria with respect to the background flow. This term is proportional to $\delta_{ij}-3d_id_j$, the same form as the term in [19] derived for ensembles of dipoles. It can be interpreted as an active stress in the notation of [20]. To obtain further insight into the rheology of bacterial suspension, we must determine P^∞.

Without loss of generality, we choose E and $\boldsymbol{\Omega}$ corresponding to planar shearing and straining flows in three cases, allowing us to calculate viscosities valid in a variety of relevant physical situations. First, we consider a pure straining flow, which has a tendency to align elongated particles and hence bacteria. Such a flow is representative of the flows bacteria would experience when swimming in groups, as they tend to align in these cases. Next, we calculate the effective viscosity for planar shearing flows. This allows for comparison with previous analytical work on the viscosity of passive suspensions that use such flows (e.g., [21,18,22]). Finally, we consider an oscillatory shear flow. This type of flow is used in experiments where viscosity is measured. The shearing and straining flows are described by E with $E_{12}=E_{21}=\frac{\dot{\gamma}}{2}$ and all other components $E_{ij}=0$ with $\Omega=(0,0,-\frac{\dot{\gamma}}{2})$ and $\Omega=(0,0,0)$, respectively. For the oscillatory case, we replace $\dot{\gamma}$ with $\dot{\gamma}\sin\omega_0 t$. We define the effective viscosity by $\hat{\eta} := \frac{\Sigma_{12}}{\dot{\gamma}}$. It is not possible to solve the Fokker-Planck equa-

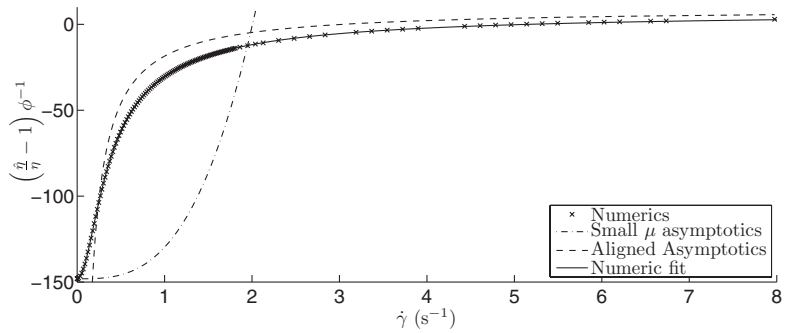

FIG. 4. $(\frac{\hat{\eta}}{\eta}-1)\phi^{-1}$ vs $\dot{\gamma}$ for the case of no vorticity [$\Omega=(0,0,0)$] evaluated numerically along with small μ asymptotics [Eq. (11)], and aligned asymptotics [Eq. (7)].

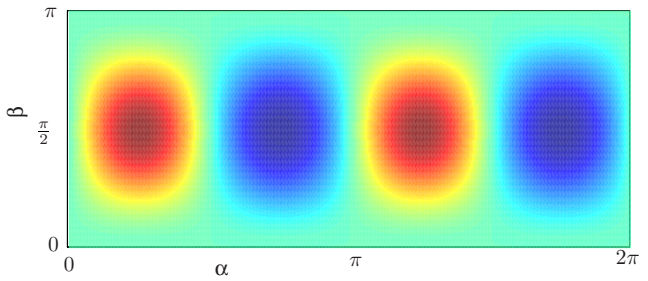

FIG. 5. (Color online) A plot of P^{∞} in the flow without vorticity for $\dot{\gamma}=0.14\ \mathrm{s}^{-1}$. Darker regions indicate the peaks and troughs. The peaks (red) are located at approximately $\alpha=\frac{\pi}{4},\frac{5\pi}{4}$ with $\beta=\frac{\pi}{2}$.

tion analytically for any of our background flows, so we must do so asymptotically in various parameters and numerically in the general case. The parameters used depend on the form of the Fokker-Planck equation for each flow. The numerics are performed using a finite difference scheme on a uniform mesh with 80,400 points. The resulting linear system is solved using the method of biconjugate gradients. Numerical viscosities are then calculated using Eq. (6) by setting the various parameters to values established in the literature. It is assumed that the bacteria have dimensions $b=4\ \mu\mathrm{m}$ (see [7]), $\frac{b}{a}=5.7$ (except for the small eccentricity asymptotics, where it is assumed that $B=0.01$) and $\lambda=0.5$. We assume a bacterial swimming speed $v=50\ \mu\mathrm{m\ s}^{-1}$ and a rotational diffusion constant $D=0.017\ \mathrm{s}^{-1}$ (see [8]).

In the planar straining flow, bacteria tend to align with the steady axis of the flow, corresponding to angles $\alpha=\frac{\pi}{4},\frac{3\pi}{4}$ with $\beta=\frac{\pi}{2}$. Plugging this into Eq. (6) and applying Eq. (3a), we calculate an effective viscosity

$$\frac{\hat{\eta}}{\eta}=1+\phi\left[S-\frac{3bv}{8a^2\dot{\gamma}}NK\right]+O(\phi^2), \tag{7}$$

where S is a scalar function of e, given in [16]. Plots of N, K, and S are given in Fig. 3. The second term in Eq. (7) represents the passive contribution and the third the active contribution. This formula extends the result of [10] to 3D. Since $K>0$, there is a decrease in the effective viscosity due to self-propulsion. Note that Eq. (7) is only valid for $\dot{\gamma}\gg D$, because the assumption of full alignment is invalid otherwise. Equation (7) is plotted against $\dot{\gamma}$ with the corresponding numerics in Fig. 4.

For the same flow, we now assume the dimensionless parameter $\mu:=\frac{\dot{\gamma}B}{D}\ll 1$ (i.e., bacteria have a weak tendency to align with the background flow due to being nearly spherical or weak advection). In this flow, the deterministic part of the particle trajectories is described by

$$\begin{cases}\dot{\alpha}^D=\dfrac{B\dot{\gamma}}{2}\cos 2\alpha\\ \dot{\beta}^D=\dfrac{B\dot{\gamma}}{4}\sin 2\alpha\sin 2\beta\end{cases}. \tag{8}$$

Constructing $\dot{\hat{d}}^D$ from this and plugging these into $\frac{\partial P^{\infty}}{\partial t}=0$ (see Eq. (4)) leads to the steady-state Fokker-Planck equation

$$0=\frac{\mu}{2}\sin 2\alpha\sin\beta\left(3P^{\infty}\sin\beta-\frac{\partial P^{\infty}}{\partial\beta}\cos\beta\right)-\frac{\mu}{2}\cos 2\alpha\frac{\partial P^{\infty}}{\partial\alpha}+\Delta_{\alpha,\beta}P^{\infty}, \tag{9}$$

where $\Delta_{\alpha,\beta}$ is the spherical laplacian. For $\mu\ll 1$, we calculate an asymptotic solution to the Fokker-Planck equation, given by

$$P^{\infty}=\frac{1}{4\pi}\left[1+\mu\frac{1}{4}\sin 2\alpha\sin^2\beta\right]+O(\mu^2). \tag{10}$$

A plot of a numerical solution for P^{∞} is given in Fig. 5. Plugging Eq. (10) into Eq. (6) and applying Eq. (3a), we derive the effective viscosity

$$\frac{\hat{\eta}}{\eta}=1+\phi\left[M-\frac{3b}{80a^2\dot{\gamma}}NKv\mu+O(\mu^2)\right]+O(\phi^2), \tag{11}$$

where M is a scalar function of e given in [16]. Plots of M, N, and K are given in Fig. 3. The second term is the passive contribution and the third term is the active contribution. This formula indicates that the suspension is very weakly non-Newtonian (since $\hat{\eta}=C+O(\dot{\gamma}^2)$). A striking feature of the formula is the fact that the active contribution does not disappear in the limit $\dot{\gamma}\to 0$. This is counterintuitive because as $\dot{\gamma}\to 0$, $P^{\infty}\to\frac{1}{4\pi}$ and hence the active contribution to the bulk deviatoric stress Σ^a averages to zero. However, for small $\dot{\gamma}$, $P^{\infty}=\frac{1}{4\pi}+C\dot{\gamma}+\ldots$ and Σ^a acquires a contribution $\propto\dot{\gamma}$. When calculating Σ^a from P^{∞}, the constant term (in $\dot{\gamma}$) averages to zero, but the linear term remains. Hence, the active contribution to the effective viscosity $\hat{\eta}^a:=\frac{\Sigma^a}{\dot{\gamma}}$ contains a nonvanishing term. However, in reality, the time it takes for a suspension to reach the steady state P^{∞} increases as $\dot{\gamma}\to 0$. Thus, for small enough $\dot{\gamma}$, diffusion will dominate advection and the actual P^{∞} will be closer to $\frac{1}{4\pi}$, which will produce

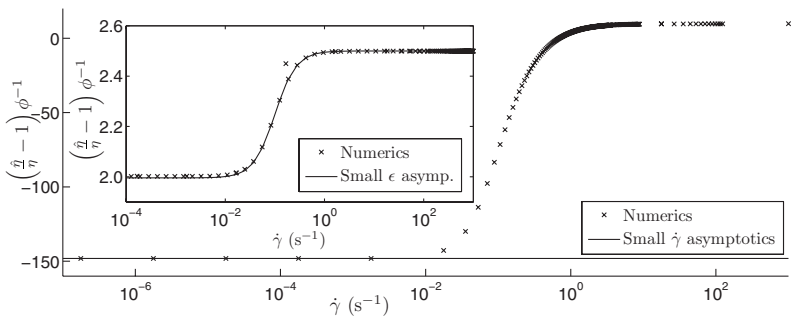

FIG. 6. $(\frac{\hat{\eta}}{\eta}-1)\phi^{-1}$ vs $\dot{\gamma}$ for the case with vorticity. The inset is for $B=\frac{b^2-a^2}{b^2+a^2}=.01$ along with small $\epsilon=\frac{b}{a}-1$ asymptotics [Eq. (15)], while the main plot is for $\frac{b}{a}=5.7$ along with small $\frac{\dot{\gamma}}{D}$ asymptotics [Eq. (19)].

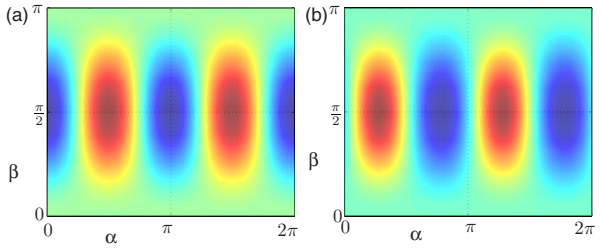

FIG. 7. (Color online) (a) A plot of P^{∞} in the flow with vorticity for $B=\frac{b^2-a^2}{b^2+a^2}=.01$ and $\dot{\gamma}=0.017\ s^{-1}$. Darker regions indicate the peaks and troughs. The peaks (red) are located at approximately $\alpha=\frac{\pi}{2},\frac{3\pi}{2}$ with $\beta=\frac{\pi}{2}$. (b) A plot of P^{∞} in the flow with vorticity for $\frac{b}{a}=5.7$ and $\dot{\gamma}=0.14\ s^{-1}$. Darker regions indicate the peaks and troughs. The peaks (red) are located at approximately $\alpha=\frac{\pi}{4},\frac{5\pi}{4}$ with $\beta=\frac{\pi}{2}$.

$\hat{\eta}'=0$. Equation (11) is plotted against $\dot{\gamma}$ along with corresponding numerics in Fig. 4.

We next consider the planar shear flow. In this flow, the deterministic part of the spheroids' orbits is described by

$$\begin{cases} \dot{\alpha}^D = \dfrac{\dot{\gamma}}{2}(1 + B\cos 2\alpha) \\ \dot{\beta}^D = \dfrac{B\dot{\gamma}}{4}\sin 2\alpha \sin 2\beta. \end{cases} \tag{12}$$

Plugging this into $\frac{\partial P^{\infty}}{\partial t}=0$ (see Eq. (4)) yields the Fokker-Planck equation

$$0 = \frac{B\dot{\gamma}}{2}\sin 2\alpha \sin\beta\left(3P^{\infty}\sin\beta - \frac{\partial P^{\infty}}{\partial\beta}\cos\beta\right) - \frac{\dot{\gamma}}{2}(1 + B\cos 2\alpha)\frac{\partial P^{\infty}}{\partial\alpha} + D\Delta_{\alpha,\beta}P^{\infty}. \tag{13}$$

P^{∞} has been calculated for small eccentricity e asymptotically in the small parameter $\epsilon := \frac{b}{a}-1$ in [18], and is given by

$$P^{\infty} = \frac{1}{4\pi}\left[1 + \epsilon\frac{3\sin^2\beta\sin\left(2\alpha - \arctan\frac{\dot{\gamma}}{6D}\right)}{2\sqrt{1+\left(\frac{6D}{\dot{\gamma}}\right)^2}}\right] + O(\epsilon^2). \tag{14}$$

A plot of a numerical solution for P^{∞} is given in Fig. 7. Plugging Eq. (14) into Eq. (6) and applying Eq. (3a) produces

$$\frac{\hat{\eta}}{\eta} = 1 + \phi\left[\frac{5}{2} - \frac{27vbDN(5\lambda^2+10\lambda+2)}{10a^2(36D^2+\dot{\gamma}^2)(1+\lambda)^4}\epsilon + O(\epsilon^2)\right] + O(\phi^2). \tag{15}$$

The second and third terms are the passive and active contribution, respectively. As in [18], the effect due to eccentricity differs from that of a sphere at $O(\epsilon^2)$. Equation (15) is plotted against $\dot{\gamma}$ along with corresponding numerics in Fig. 6.

We now place our particles in a weak ($\frac{\dot{\gamma}}{D}\ll 1$) oscillatory shear flow with frequency ω_0. In this flow, the deterministic particle trajectories will obey

$$\begin{cases} \dot{\alpha}^D = \dfrac{\dot{\gamma}}{2}\sin\omega^0 t(1 + B\cos 2\alpha) \\ \dot{\beta}^D = \dot{\gamma}\sin\omega^0 t\dfrac{B}{4}\sin 2\alpha \sin 2\beta \end{cases}. \tag{16}$$

Using these to construct $\dot{\hat{d}}^D$ and plugging them into (4) yields the time-dependent Fokker-Planck equation

$$\frac{\partial P}{\partial t} = \frac{1}{2}\dot{\gamma}\sin\omega^0 t\left[B\sin 2\alpha\sin\beta\left(3P\sin\beta - \frac{\partial P}{\partial\beta}\cos\beta\right) - (1 + B\cos 2\alpha)\frac{\partial P}{\partial\alpha}\right] + D\Delta_{\alpha,\beta}P. \tag{17}$$

We calculate the solution to Eq. (17) asymptotically in $\frac{\dot{\gamma}}{D}$ by expanding it in a Fourier series, producing

$$P(\alpha,\beta,t) = \frac{3}{8\pi}\frac{\dot{\gamma}BD\sin 2\alpha\sin^2\beta 6D\sin\omega^0 t}{36D^2+(\omega^0)^2} + \cdots \tag{18}$$

A plot of a numerical solution for P^{∞} is given in Fig. 7. Plugging Eq. (18) into Eq. (6) and applying Eq. (3a) yields

$$\frac{\hat{\eta}}{\eta} = 1 + \phi\left[M - K\frac{27bvBDN}{20a^2(36D^2+(\omega^0)^2)}\right] + \ldots \tag{19}$$

The second and third terms are the passive and active contributions, respectively. Equation (19) is plotted against $\dot{\gamma}$ along with corresponding numerics in Fig. 6.

We have calculated the effective viscosity of bacterial suspension and performed experiments in qualitative agreement. The dilute limit allowed us neglect the interactions between bacteria and thus to carry out the calculations fully analytically. While it is not obvious that the interactions are negligible in experiments, the results are nevertheless in qualitative agreement with experiment. We have demonstrated and observed that bacterial self-propulsion decreases the effective viscosity of an ambient fluid. For weak enough background flows, this decrease outweighs the passive increase in viscosity due to the suspension to produce a net decrease in the viscosity of the fluid. For strong background flows the effect of self-propulsion becomes negligible and an active suspension becomes indistinguishable from a passive one.

The reduction in viscosity due to self-propulsion predicted in our model relies on the bacteria being "pushers" (i.e., $c>0$). However, our results are still valid for "pullers" (e.g., some motile algae) which can be modeled in the same way but with $c<0$. In this case, there is an increase in viscosity due to self-propulsion. That there is a fundamental difference in the physics of "pushers" and "pullers" was previously observed in [23,24].

The work of I. S. Aranson, A. Sokolov, and D. Karpeev was supported by the DOE (Grant No. DE-AC02–06CH11357). The work of B. Haines and L. Berlyand was supported by the DOE Grant No. DE-FG02–08ER25862 and NSF (Grant No. DMS-0708324).

APPENDIX: THE BULK STRESS

We calculate Σ by splitting it into passive, tumbling, and active contributions. We write $\boldsymbol{u}^d=\boldsymbol{u}^p+\boldsymbol{u}^t+\boldsymbol{u}^a$, where $\boldsymbol{u}^p$ describes interaction of a passive spheroid with the background flow, $\boldsymbol{u}^t$ describes the effects of tumbling, and $\boldsymbol{u}^a$ describes the effects of forward self-propulsion. We then define Σ^p, Σ^t, and Σ^a as the corresponding bulk stress.

Σ^p is calculated in [17] and is given by

$$\Sigma_{ij}^p = 2\eta E_{ij} + \frac{5b^2}{a^2}\phi\eta\int_{S^2}\Lambda_{ijkl}P^\infty dSE_{kl} - 3\eta\phi BY^H\frac{b^2}{a^2}\int_{S^2}(\epsilon_{ikl}d_j + \epsilon_{jkl}d_i)d_l\epsilon_{kmn}d_md_nP^\infty dSE_{mn}, \tag{A1}$$

where ϕ is the volume fraction of the suspension and Y^H and Λ_{ijkl} are functions of e given in [16]. A plot of Y^H is given in Fig. 3. Σ^t is calculated in [18] [1] and is given by

$$\Sigma_{ij}^t = 3\eta\phi Y^H\frac{b^2}{a^2}D\int_{S^2}(\epsilon_{ikl}d_j + \epsilon_{jkl}d_i)d_l\epsilon_{kmn}d_m(\partial_nP^\infty)dS. \tag{A2}$$

It remains to calculate Σ^a. We do this by further decomposing $\boldsymbol{u}^a$ by writing $\boldsymbol{u}^a=\boldsymbol{u}^{a,1}+\boldsymbol{u}^{a,2}+\boldsymbol{u}^{a,3}$, where

$$\begin{cases} \eta\Delta\boldsymbol{u}^{a,1} = \nabla p^{a,1} + c\hat{\boldsymbol{d}}\delta(\boldsymbol{x}-\boldsymbol{x}^f) & \boldsymbol{x}\in\mathbb{R}^3 \\ \nabla\cdot\boldsymbol{u}^{a,1} = 0 & \boldsymbol{x}\in\mathbb{R}^3 \\ \boldsymbol{u}^{a,1}\to 0 & \boldsymbol{x}\to\infty, \end{cases} \tag{A3}$$

$$\begin{cases} \eta\Delta\boldsymbol{u}^{a,2} = \nabla p^{a,2} & \boldsymbol{x}\in\mathbb{R}^3\setminus B \\ \nabla\cdot\boldsymbol{u}^{a,2} = 0 & x\in\mathbb{R}^3\setminus B \\ \boldsymbol{u}^{a,2} = -\boldsymbol{u}^{a,1} & x\in\partial B \\ \boldsymbol{u}^{a,2}\to 0 & \boldsymbol{x}\to\infty \end{cases}, \tag{A4}$$

and

$$\begin{cases} \eta\Delta\boldsymbol{u}^{a,3} = \nabla p^{a,3} & \boldsymbol{x}\in\mathbb{R}^3\setminus B \\ \nabla\cdot\boldsymbol{u}^{a,3} = 0 & \boldsymbol{x}\in\mathbb{R}^3\setminus B \\ \boldsymbol{u}^{a,3} = \boldsymbol{v}^a & \boldsymbol{x}\in\partial B \\ \boldsymbol{u}^{a,3}\to 0 & \boldsymbol{x}\to\infty \\ \displaystyle\int_{\partial B}(\sigma^{a,1}+\sigma^{a,2}+\sigma^{a,3})\cdot\hat{v}dx + c\hat{\boldsymbol{d}} = 0. \end{cases} \tag{A5}$$

$\boldsymbol{u}^{a,3}$ is the flow due to a translating spheroid and $\boldsymbol{u}^{a,1}$ is a force monopole, both of which produce no bulk stress. The bulk stress due to $\boldsymbol{u}^{a,2}$ can be calculated without actually solving the problem by applying Faxén's law for prolate spheroids (see [17]),

$$\Sigma_{ij}^{a,2}(\hat{\boldsymbol{d}}) = -\frac{5}{2e^3}\pi\eta\Lambda_{ijkl}\int_{-be}^{be}((be)^2-v^2)\left[1+((be)^2 - v^2)\frac{1-e^2}{8e^2}\Delta\right]\left(\frac{\partial u_k^{a,1}}{\partial x_l}+\frac{\partial u_l^{a,1}}{\partial x_k}\right)\Big|_{\hat{\boldsymbol{d}}v}dv. \tag{A6}$$

Performing the integration in Eq. (A6) and averaging over orientations, we get

$$\Sigma_{ij}^a = \Sigma_{ij}^{a,2} = \frac{c}{16\pi a^2}\phi K\int_{S^2}(\delta_{ij}-3d_id_j)P^\infty dS, \tag{A7}$$

where K is given in [16]. A plot of K is given in Fig. 3.

Combining Eqs. (A1), (A2), and (A7), we get Eq. (6).

[1] The stress due to tumbling in our model is equivalent to the diffusive stress due to the Brownian motion of fluid particles calculated in [18]. This is because both effects produce bulk hydrodynamic stress through the random rotation of the particle $\boldsymbol{\omega}^R$, which is equal in both cases.

[1] X.-L. Wu and A. Libchaber, Phys. Rev. Lett. **84**, 3017 (2000).
[2] M. J. Kim and K. S. Breuer, Phys. Fluids **16**, 78 (2004).
[3] C. Dombrowski, L. Cisneros, S. Chatkaew, R. E. Goldstein, and J. O. Kessler, Phys. Rev. Lett. **93**, 098103 (2004).
[4] I. H. Riedel, K. Kruse, and J. Howard, Science **309**, 300 (2005).
[5] J. Buhl *et al.*, Science **312**, 1402 (2006).
[6] D. Saintillan and M. J. Shelley, Phys. Rev. Lett. **100**, 178103 (2008).
[7] A. Sokolov, I. S. Aranson, J. O. Kessler, and R. E. Goldstein, Phys. Rev. Lett. **98**, 158102 (2007).
[8] A. Sokolov and I. S. Aranson, Phys. Rev. Lett. **103**, 148101 (2009).
[9] Y. Hatwalne, S. Ramaswamy, M. Rao, and R. A. Simha, Phys. Rev. Lett. **92**, 118101 (2004).
[10] B. M. Haines, I. S. Aranson, L. Berlyand, and D. A. Karpeev, Phys. Biol. **5**, 046003 (2008).
[11] T. Ishikawa and T. J. Pedley, J. Fluid Mech. **588**, 399 (2007).
[12] M. E. Cates, S. M. Fielding, D. Marenduzzo, E. Orlandini, and J. M. Yeomans, Phys. Rev. Lett. **101**, 068102 (2008).
[13] H. C. Berg and D. A. Brown, Nature (London) **239**, 500 (1972).
[14] L. Turner, W. S. Ryu, and H. C. Berg, J. Bacteriol. **182**, 2793 (2000).
[15] M. Wu, J. W. Roberts, S. Kim, D. L. Koch, and M. P. Delisa, Appl. Environ. Microbiol. **72**, 4987 (2006).
[16] See EPAPS Document No. E-PLEEE8-80-113910 for table of

functions. For more information on EPAPS, see http://www.aip.org/pubservs/epaps.html.
[17] S. Kim and S. Karrila, *Microhydrodynamics* (Dover Publications, New York, 1991).
[18] E. J. Hinch and L. G. Leal, J. Fluid Mech. **52**, 683 (1972).
[19] R. A. Simha and S. Ramaswamy, Phys. Rev. Lett. **89**, 058101 (2002).
[20] K. Kruse, J. F. Joanny, F. Jülicher, J. Prost, and K. Sekimoto, Phys. Rev. Lett. **92**, 078101 (2004).
[21] G. B. Jeffery, Proc. R. Soc. London, Ser. A **102**, 161 (1922).
[22] L. G. Leal and E. J. Hinch, J. Fluid Mech. **46**, 685 (1971).
[23] J. P. Hernandez-Ortiz, C. G. Stoltz, and M. D. Graham, Phys. Rev. Lett. **95**, 204501 (2005).
[24] V. T. Gyrya, I. S. Aranson, L. V. Berlyand, and D. A. Karpeev, Bull Math. Biol., doi: 10.1007/s11538–009–9442–6 (2009).